

MBE obtained n-CdO:Eu/p-Si heterojunctions - electron beam induced profiling, electrical and structural properties

Ewa Przeździecka^{1,*}, Igor Perlikowski², Dawid Jarosz³, Sergij Chusnutdinow¹, Aleksandra Wierzbicka¹, Abinash Adhikari^{1,4}, Marcin Stachowicz¹, Rafał Jakiela¹, Eunika Zielony², Piotr Wojnar^{1,5}, A. Kozanecki¹

* Correspondence: eilczuk@ifpan.edu.pl (E.P.)

Keywords: Semiconductors, Cadmium oxide, PN diode, Heterostructures, Electron beam induced current, Scanning electron microscopy, Molecular Beam Epitaxy

Highlights

1. XRD patterns reveal that the films have cubic structure with polycrystalline nature.
2. Electron beam induced currents reveal of p-n junction on the CdO and Si interface.
3. The diffusion length of minority carriers were obtained.

Abstract

The present investigation reports on the fabrication and characterization of heterojunctions based on in-situ Eu-doped CdO layers, which were deposited on p-type silicon using the plasma-assisted molecular beam epitaxy (PA-MBE) method. The structural and optical properties of the cadmium oxide (CdO) films were investigated using X-ray diffraction and Fourier transform infrared spectroscopy (FTIR). The CdO:Eu films are polycrystalline. The electrical properties of the *p-n* heterojunction composed of transparent *n*-CdO:Eu and *p*-Si semiconductors were investigated by current-voltage and electron beam-induced current (EBIC) measurements. Current-voltage measurements demonstrate good junction characteristics with a rectifying ratio of ~ 20 at ± 3 V. EBIC measurements allowed us to calculate the diffusion length of minority carriers and the precise location of the depleted area at the CdO and Si interfaces.

1. Introduction

Semiconductors based on metal oxides have been studied widely for electronic devices such as solar cells, gas sensors, liquid crystal display, smart windows, flat panel display, optical heaters and light emitting diodes[1,2]. Cadmium oxide (CdO), which is metal-oxide-semiconductor is one of the promising materials for realizing optoelectronic devices [3]. Cadmium oxide is an n-type semiconductor due to oxygen vacancies and has a rock-salt crystalline structure[4–7]. CdO which possesses a direct band gap of 2.3 eV will be a useful material in the optoelectronic applications by making heterojunctions with Si[8,9] GaN [8,9] and CdS[10] and with others *p*-type materials. Many of growth techniques such as sol-gel[11,12], RF sputtering[4,13,14] pulsed laser deposition[15–17], chemical bath deposition[18,19] and molecular beam epitaxy[7,20] have been used to prepare CdO thin films.

Cadmium oxide thin films have usually *n*-type character and interestingly it is possible to tune the electron concentration and mobility in the orders of magnitude by playing with the

growth parameters and the stoichiometry of the layers in particular, by manipulating the oxygen deficiency. Understanding of the electrical parameters of CdO layers is crucial for their future applications[4,5,7,21,22] In the case of heterostructures for diodes, it is also important to understand the transport mechanisms at the interface between the *p*-type material and the *n*-type material. The quality of the interface is critical to the transport mechanism and the quality of the diodes[23]. Doping of the layers also affects their physical properties, including electrical properties as was previously observe in the doped CdO layers. [3,15,24–31] To clarify the carrier transport mechanism in *n*-CdO:Eu/*p*-Si junction obtained by MBE, we have investigated the electron-beam-induced current. In particular Eu impact on the minority carrier diffusion length was investigated in this work and the location of junction on the interface was confirmed.

2. Experimental

2.1 Materials

A series of heterojunctions based on *n*-type Eu-doped CdO layers grown on commercially available *p*-type (100) Si substrates was obtained using the Riber Compact 21B plasma-assisted molecular beam epitaxy (PA-MBE) system. High-purity Cadmium (6N) and Europium (4N) served as sources for Cd and Eu, respectively, within the effusion cells, whereas an oxygen plasma source powered by radio frequency (RF) power was used as a source of oxygen in the MBE setup. Preceding the growth process, the Si (001 oriented) substrates were chemically etched using Buffered Oxide Etch (BOE) for 2 minutes followed by subsequent wet and dry cleaning using deionized water and N₂ gas respectively. Then the Si substrates were subjected to annealing within the load chamber of the MBE system at a temperature of 150°C for 1 hour, prior to their transfer to the growth chamber. During the growth, the Cd flux was maintained at approximately 2.2×10^{-7} Torr controlled by fixing the Cd effusion cell temperature at 380°C. Meanwhile, the Eu flux was varied from 5.6×10^{-9} Torr to 5.0×10^{-9} Torr by changing the temperature of the Eu effusion cell (ranging from 300°C to 380°C in increments of 20°C). The growth process was carried out at a temperature of 360°C measured by thermocouple located close to the sample. The oxygen flow was at the level of 3 sccm at a fixed 400W RF power of the oxygen plasma throughout the growth process.

2.2 Experimental techniques

The structural analysis of CdO layers doped *in situ* with Eu was carried out using X-ray diffraction (XRD). A Panalytical X'Pert Pro-MRD diffractometer was utilized, featuring a hybrid two-bounce Ge (220) monochromator coupled with an X-ray mirror and a threefold Ge (220) analyzer positioned in frpont of a Pixel detector or proportional detector. All measurements were performed using Cu_{Kα1} radiation with a wavelength of 1.5406 Å.[32,33]

The current voltage (I-V) characteristics are the most important measurements to study the electrical behavior of any diode. I-V measurements were performed using a computer controlled Keithley 4200-SCS semiconductor characterization system in dark. Minority carrier diffusion length measurements were conducted on the structures which were cleaved *in situ* perpendicular to the growth plane in the ZEISS EVO HD15 Scanning Electron Microscope (SEM), using the Digital Image Scanning System (DISS 5) Electron-beam-induced current (EBIC) in the microscope chamber under a 10 kV electron beam accelerating voltage.

FTIR measurements were carried out with infrared spectrometer FTIR Vertex 70v from Bruker equipped with Platinum ATR (Attenuated Total Reflectance) add-on. The samples were placed on the crystal surface and kept in good optical contact, the measurements were performed in vacuum. The background spectra of a blank diamond were used to generate absorption spectra. The acquisition of signal was performed with LN-MCT (HgCdTe) detector cooled with nitrogen. The scan frequency was set to 10 kHz in range of 400-4000 cm⁻¹ of the mid-infrared lamp as a emission source. Additionally, a series of experimentation has been performed with Bruker infrared microscope FTIR Lumos II on three selected surface spots of each sample. The 8x objective provides magnification, while the two measurement modes (reflection and ATR) enable the study of both bulk and surface properties of the sample. The ZnSe beam splitter is used to separate the incident and reflected beams in the microscope.

The ATR technique utilizes the phenomenon of total internal reflection, which allows for non-destructive analysis of samples without the need for sample preparation. The diamond crystal in the Platinum ATR accessory enhances the intensity of the reflected light, improving the sensitivity of the measurements. The LN-MCT detector, cooled with liquid nitrogen, provides high-sensitivity and low-noise detection in the mid-infrared range.

3. Results and discussion

3.1 Structural analysis

The XRD patterns of Eu-doped CdO layers grown on Si (100) substrates are shown in Fig 1. The 400 diffraction peak at about 69° corresponds to the silicon substrate and is clearly distinguishable. The diffraction peak at (2θ) about 33°, 38.3°, 55.2°, 65.9°, 81.9°, 91.3° and 94.4° attributed respectively to the 111, 200, 220, 311, 400, 331, and 420 diffraction peaks of CdO cubic rocksalt structure (JCPDF card no. 00-005-0640). All the grown layers are polycrystalline and part of them with the preferred growth direction being expressed in terms of texture coefficient (TC) defined as[34],

$$TC(h, k, l) = \frac{\frac{I(h, k, l)}{I_o(h, k, l)}}{\frac{1}{n} \sum \frac{I(h, k, l)}{I_o(h, k, l)}}$$

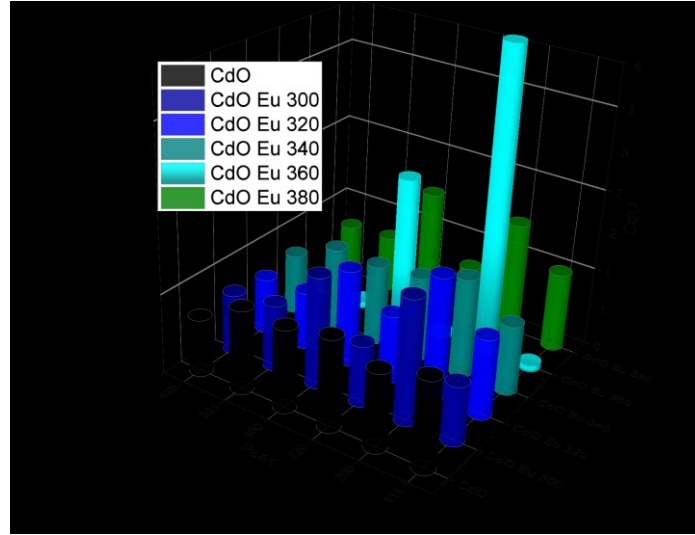
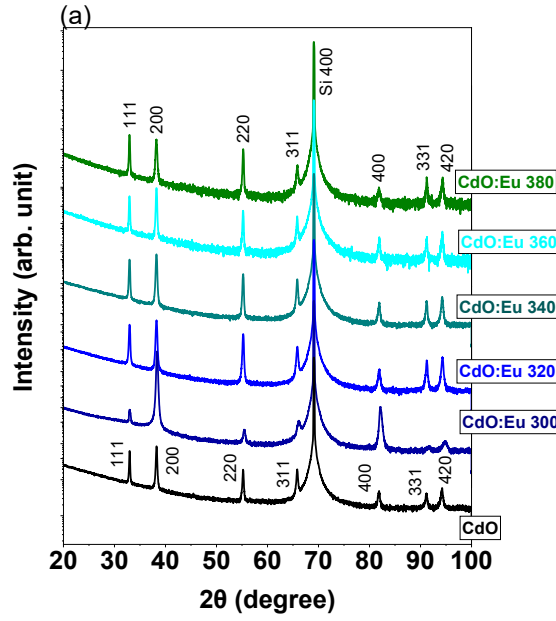


Figure 1. (a) XRD patterns of CdO/*p*-Si films in situ doped with Eu grown by MBE. (b) texture coefficient (TC) analysis for all the X-ray CdO peaks observed in part (a).

where I and I_o are the intensity of diffraction peak and standard intensity based on (JCPDF card no. 00-005-0640) of the hkl plane, respectively. The total number of diffraction peaks observed, denoted as n , is 6 in the present study. Consequently, the maximum possible value of TC is 6. The calculated value of TC corresponding to all peaks are presented on Fig 1 (b). According to the definition, a TC value close to 1 suggests a randomly oriented layer, while a TC value close to 6 indicates a perfectly oriented layer. TC values greater than 1 suggest a predominance of grains aligned in a specific hkl direction. Conversely, values between 0 and 1 indicate a scarcity of grains oriented in that direction [35,36]. The TC values of pure CdO are close to 1 and it increases for 200 peak with an increase in Eu dopant concentration in CdO. In the present study, the highest TC value of 3.788 is obtained for 002 peak for sample CdO:Eu360. This increase in TC value with increasing Eu dopant concentration indicates that the grains are preferentially aligned along the [100] direction. The grain size corresponding to the 200 diffraction peak is determined using Scherrer's relation [37] and listed in Table 1. The grain size of pure CdO is

found to be 27.83 nm. The grain size increases with an increase in Eu doping concentration in the CdO lattice and found to be in the range of 29-39 nm.

Table 1. Bragg angle (2θ), FWHM, grain size, and texture coefficient TC of 200 diffraction peak of CdO and Eu-doped CdO layers

	(2θ)₂₀₀ (in degree)	FWHM (in degree)	D₂₀₀ (in nm)	TC₂₀₀
CdO	38.21	0.30	27.83	0.965
CdO:Eu300	38.23	0.23	36.88	1.544
CdO:Eu320	38.23	0.25	33.35	1.527
CdO:Eu340	38.23	0.27	30.89	1.248
CdO:Eu360	38.35	0.26	32.34	3.788
CdO:Eu380	38.25	0.22	38.38	1.442

3.2 Fourier transform infrared spectroscopy

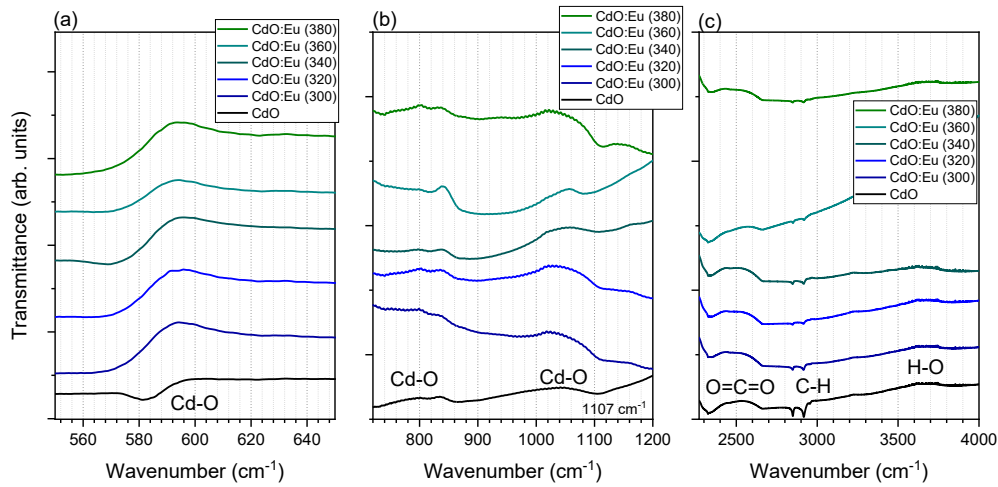


Figure 2. FTIR Transmittance spectra at room temperature.

To study characteristic functional groups observed in the samples, Fourier transform infrared spectroscopy (FTIR) spectra were recorded in the range of 500-4000 cm^{-1} as presented in Fig. 2. For CdO samples the absorption band around 581 cm^{-1} and 839 cm^{-1} and band at about 1117 cm^{-1} [38] (Fig 2 (a) and 2 (b)) corresponds to (Cd-O) and confirm the formation of CdO thin film[39]. These line is observed in all the samples, but the shape of the spectrum minority changes with Eu concentration. The broad FTIR absorption band at 3500 -3700 cm^{-1} is assigned to stretching vibrational mode of a hydroxyl group O- H [39,40]. [38,39] it was also suggested that band band observed at 3612 cm^{-1} is ascribed to the symmetric stretching mode

of H–O–H [41]. The bands at 2930 cm⁻¹ are assigned to stretching modes of C–H group [42]. In the literature, the absorption bands at about ~2300 cm⁻¹ are identified as a consequence of the presence of atmospheric carbon dioxide O=C=O. FTIR bands differences modes can be due to development of lattice distortion and/or defects, associated with Eu dopant concentrations.

3.3 Electrical characterization

The diodes structures consist of 350–470 nm thick CdO or CdO:Eu layers grown by PA-MBE on commercially available *p*-type Si substrates. The europium doping was confirmed by measured secondary ion mass spectroscopy (SIMS) depth profiles. CdO itself has high carrier (electron) concentration[7], and doping with Eu further increases it[25]. Thus, expected carrier concentration on the *n*-side of the investigated junctions is at the level 1e¹⁹-1e²⁰ cm⁻³ and it is ~2·10¹⁷ cm⁻³ in the case of *p*-Si substrate. In analyzed in this paper junction rectifying factor at ±3 V is 18 for both CdO/*p*-Si and CdO:Eu/*p*-Si.

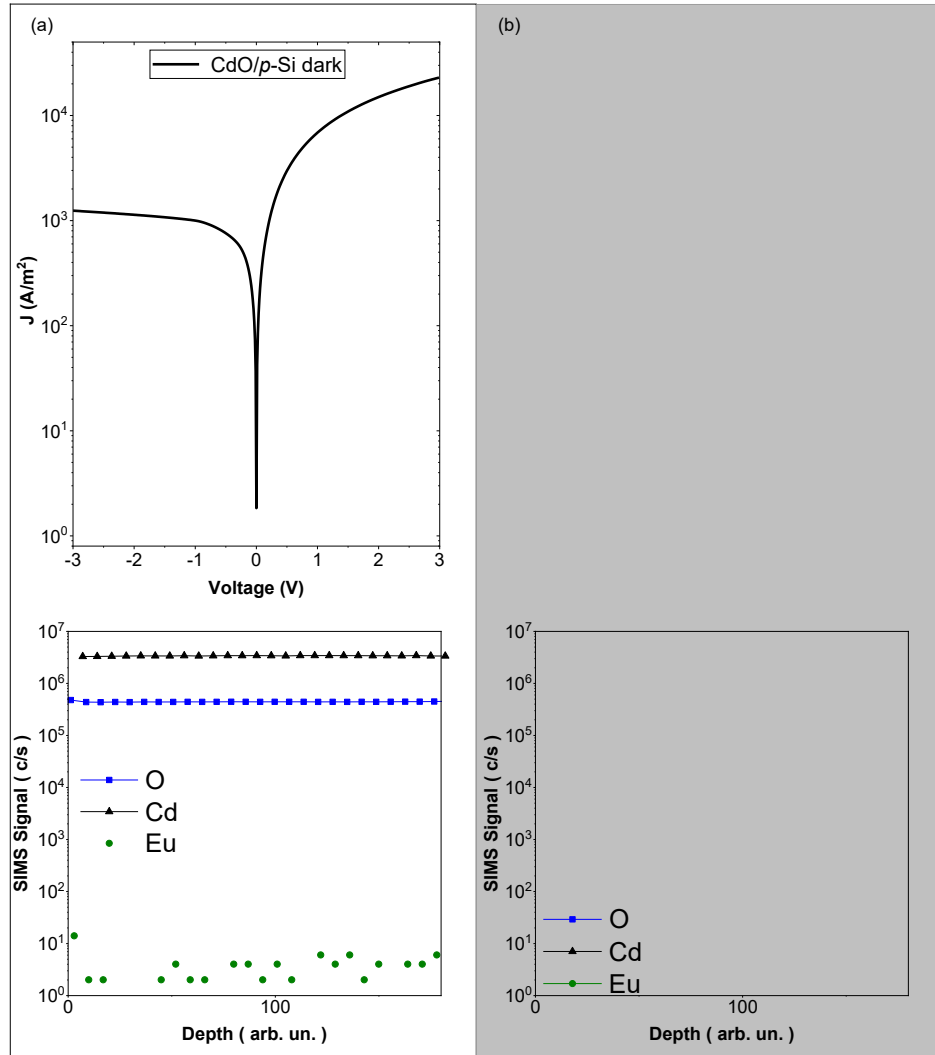


Fig 3. (a) Current density-voltage characteristics of the *n*-CdO/*p*-Si measured at 300K in the dark and SIMS depth profile for this sample (b) Current density-voltage characteristics of the *n*-CdO:Eu/*p*-Si samples measured at 300K in dark and SIMS depth profile for this sample with visible Eu doping profile.

The EBIC technique is the method of choice for determining the minority carrier diffusion length. It is based on measuring the current due to nonequilibrium carriers generated by the electron beam of the scanning electron microscope (SEM) and collected by the built-in field of the barrier. The technique can be used to determine carrier lifetime, diffusion length, defect energy levels, and surface recombination velocities. Charge collection images with simultaneously gathered SEM images reveal the location of p-n junctions, recombination sites such as dislocations and precipitates, and the presence of doping level inhomogeneity [43–47]. In Fig. 4, cross sectional SEM image of a typical CdO:Eu/Si structure cleaved perpendicular to the growth plane is presented. The EBIC signal is visible as a yellow color and also EBIC line scan has been superimposed on cross-sectional SEM image. As it is seen, the maximum EBIC signal corresponds to CdO:Eu and Si interface. The EBIC line profile presented in Figure 4 is characteristic of a p- n device. It is evident that the junctions exists on the CdO/Si interface and are continuous. The minority carrier diffusion lengths can be extracted from EBIC line scan according to the following relation:

$$I_{EBIC} = I_0 \exp(-x/L_{e,p}) \quad (1)$$

where I_{EBIC} is the EBIC signal, I_0 is a constant, x describes the position of the generating electron beam. The data fitting based on this relation is represented by the yellow curves in Figure 4.

The diffusion lengths, extracted from EBIC line scans are 100 nm and 165 nm for minority electrons for CdO and CdO:Eu layers, respectively.

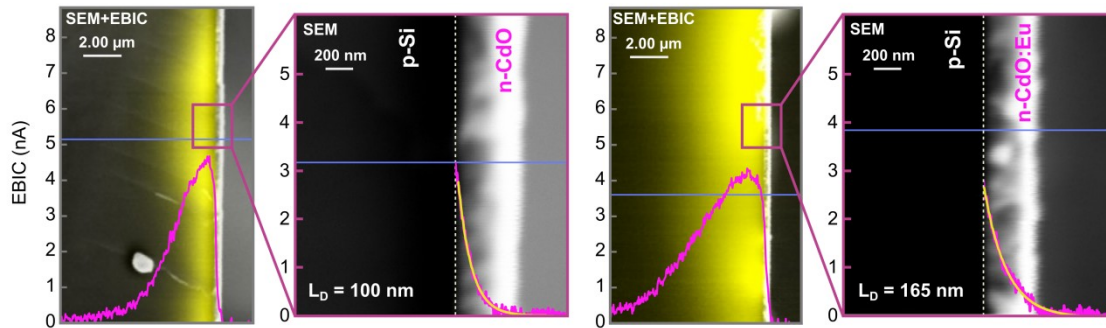


Figure 4. Cross-sectional SEM image of the CdO:Eu/Si interfaces, EBIC line scans are superimposed on the SEM image.

The diffusion length value in the previously reported oxide based structure n -MgZnO/ p -AlGaIn/GaN was 120 nm for holes in n -MgZnO and 890 nm for electrons in p -AlGaIn/GaN regions [48] while in the case of the n -ZnO/ n -GaIn structure minority carrier diffusion length was reported in the range of 125–175 nm [[49]. In case of n -CdO/electrolyte junction high value of the hole diffusion length at about 10^{-4} cm has been calculated by the Butler-Gartner equation from measurements of photocurrent quantum efficiency[50]. For example, for other structures like CuS/CdS it was 90 to 1700 nm for holes in n -type CdS and 110 to 570 for electrons in p -type CuS [51] whereas for PbSe/CdTe it was 1000 nm and 1270 nm for minority holes and electrons, respectively[52]. In conventional p–n junctions, a long minority carrier diffusion length is essential; thus, good-quality, well-ordered semiconductors are required to produce high-quality junctions. In our case, we observe a higher carrier diffusion length in CdO layers

doped with Eu, which can be correlated with the preferential orientation observed in these CdO:Eu layers.

Conclusions

Thin films of cadmium oxide (CdO) doped with Eu were prepared by plasma assisted molecular beam epitaxy on *p*-type 0001 Si substrates. The XRD diffraction patterns confirms the formation of polycrystalline CdO films in the cubic crystal structure. The peaks related to Cd–O vibrations were observed from FT-IR studies. From the electrical studies, it was observed that *p-n* junction with rectification ratio about 20 was prepared. The homogenies Eu doping in CdO layers during the epitaxy was confirmed by SIMS depth profile measurements. By applying SEM and E-BIC measurement the location of the *p-n* junction on the CdO and Si interfaces was confirmed. The minority carrier diffusion length at about 100 nm and 165 nm in case of CdO and CdO doped with Eu were respectively detected.

Conflicts of Interest: Author Ewa Przezdziecka has received research grants from the Polish National Science Center. Author Ewa Przezdziecka, Aleksandra Wierzbicka, Abinash Adhikarii and Igor Perlikowski have received an honorarium from this grant. The funders had no role in the design of the study; in the collection, analyses, or interpretation of data; in the writing of the manuscript; or in the decision to publish the results

The authors declare that they have no known competing financial interests or personal relationships that could have appeared to influence the work reported in this paper.

CRediT authorship contribution statement

Ewa Przezdziecka: Conceptualization, Funding acquisition, Supervision, Project administration, Writing – original draft. **Igor Perlikowski:** Formal analysis, Investigation, Visualization, Writing – review and editing. **Dawid Jarosz:** Investigation. **Sergij Chusnutdinow:** Methodology, Investigation. **Aleksandra Wierzbicka:** Methodology, Investigation. **Abinash Adhikari:** Data curation, Formal analysis, Writing – original draft. **Marcin Stachowicz:** Formal analysis, Writing – original draft. **Rafał Jakiela:** Investigation. **Eunika Zielony:** Writing – review and editing, Supervision. **Piotr Wojnar:** Writing – review and editing. **Adrian Kozanecki:** Writing – review and editing.

Acknowledgments

This work was supported in part by the Polish National Science Center, Grants No. 2021/41/B/ST5/00216

Data Availability

The original contributions presented in the study are included in the article; further inquiries can be directed to the author.

References

1. You, A.; Be, M.A.Y.; In, I. UV-Visible Detector and LED Based n- ZnO / p-Si Heterojunction Formed by Electrodeposition. **2015**, 032125, doi:10.1063/1.4795737.
2. Janssen, R.A.J.; Stouwdam, J.W. Red, Green, and Blue Quantum Dot LEDs with Solution Processable ZnO Nanocrystal Electron Injection Layers. *J Mater Chem* **2008**, 18, 1889–1894, doi:10.1039/b800028j.
3. Mohanraj, K.; Balasubramanian, D.; Chandrasekaran, J.; Bose, A.C. Synthesis and Characterizations of Ag-Doped CdO Nanoparticles for P-N Junction Diode Application. *Mater Sci Semicond Process* **2018**, 79, 74–91, doi:10.1016/j.mssp.2018.02.006.
4. Sakthivel, P.; Murugan, R.; Asaithambi, S.; Karuppaiah, M.; Rajendran, S.; Ravi, G. Influence of Radiofrequency Power on Structural, Morphological, Optical and Electrical Properties of Magnetron Sputtered CdO: Sm Thin Films as Alternative TCO for Optoelectronic Applications. *J Alloys Compd* **2018**, 765, 146–157, doi:10.1016/j.jallcom.2018.06.215.
5. Bhosale, C.H.; Kambale, A. V.; Kokate, A. V.; Rajpure, K.Y. Structural, Optical and Electrical Properties of Chemically Sprayed CdO Thin Films. *Mater Sci Eng B Solid State Mater Adv Technol* **2005**, 122, 67–71, doi:10.1016/j.mseb.2005.04.015.
6. Zhao, Z.; Morel, D.L.; Ferekides, C.S. Electrical and Optical Properties of Tin-Doped CdO Films Deposited by Atmospheric Metalorganic Chemical Vapor Deposition. *Thin Solid Films* **2002**, 413, 203–211, doi:10.1016/S0040-6090(02)00344-9.
7. Adhikari, A.; Wierzbicka, A.; Adamus, Z.; Lysak, A.; Sybilski, P.; Jarosz, D.; Przewdzicka, E. Correlated Carrier Transport and Optical Phenomena in CdO Layers Grown by Plasma-Assisted Molecular Beam Epitaxy Technique. *Thin Solid Films* **2023**, 780, 139963, doi:10.1016/j.tsf.2023.139963.
8. Al-Maiyaly, B.K.H. Characterization of N-CdO: Mg/p-Si Heterojunction Dependence on Annealing Temperature. *Ibn AL-Haitham Journal For Pure and Applied Science* **2017**, 29, 14–25.
9. Karataş, Ş.; Yakuphanoglu, F. Effects of Illumination on Electrical Parameters of Ag/n-CdO/p-Si Diode. *Mater Chem Phys* **2013**, 138, 72–77, doi:10.1016/j.matchemphys.2012.10.038.
10. Park, B.H.; Lee, J.; Park, H.; Do, J.Y.; Kim, Y.; Chava, R.K.; Kang, M. Effective Charge Separation through the Sulfur Vacancy Interfacial in N-CdO/p-CdS Bulk Heterojunction Particle and Its Solar-Induced Hydrogen Production. *Journal of Industrial and Engineering Chemistry* **2020**, 91, 149–166, doi:10.1016/j.jiec.2020.07.049.
11. Carballada-Galicia, D.M.; Castanedo-Pérez, R.; Jiménez-Sandoval, O.; Jiménez-Sandoval, S.; Torres-Delgado, G.; Zúñiga-Romero, C.I. High Transmittance CdO Thin Films Obtained by the Sol-Gel Method. *Thin Solid Films* **2000**, 371, 105–108, doi:10.1016/S0040-6090(00)00987-1.
12. Maity, R.; Chattopadhyay, K.K. Synthesis and Characterization of Aluminum-Doped CdO Thin Films by Sol-Gel Process. *Solar Energy Materials and Solar Cells* **2006**, 90, 597–606, doi:10.1016/j.solmat.2005.05.001.

13. Zhou, Q.; Ji, Z.; Hu, B. Bin; Chen, C.; Zhao, L.; Wang, C. Low Resistivity Transparent Conducting CdO Thin Films Deposited by DC Reactive Magnetron Sputtering at Room Temperature. *Mater Lett* **2007**, *61*, 531–534, doi:10.1016/j.matlet.2006.05.004.
14. Subramanyam, T.K.; Rao, G.M.; Uthanna, S. Process Parameter Dependent Property Studies on CdO Films Prepared by DC Reactive Magnetron Sputtering. **2001**, *69*, 133–142.
15. Gupta, R.K.; Ghosh, K.; Patel, R.; Kahol, P.K. Highly Conducting and Transparent Ti-Doped CdO Films by Pulsed Laser Deposition. *Appl Surf Sci* **2009**, *255*, 6252–6255, doi:10.1016/j.apsusc.2009.01.091.
16. Highly Conducting and Transparent Ti-Doped CdO Films by Pulsed Laser Deposition - ScienceDirect Available online: <https://www.sciencedirect.com/science/article/pii/S0169433209001275> (accessed on 10 January 2020).
17. Zheng, B.J.; Lian, J.S.; Zhao, L.; Jiang, Q. Optical and Electrical Properties of In-Doped CdO Thin Films Fabricated by Pulse Laser Deposition. *Appl Surf Sci* **2010**, doi:10.1016/j.apsusc.2009.11.049.
18. Bulakhe, R.N.; Lokhande, C.D. Chemically Deposited Cubic Structured CdO Thin Films: Use in Liquefied Petroleum Gas Sensor. *Sens Actuators B Chem* **2014**, *200*, 245–250, doi:10.1016/j.snb.2014.04.061.
19. Reddy, K.T.R.; Shanthini, G.M.; Johnston, D.; Miles, R.W. Highly Transparent and Conducting CdO Films Grown by Chemical Spray Pyrolysis. *Thin Solid Films* **2003**, *427*, 397–400, doi:10.1016/S0040-6090(02)01183-5.
20. Ashrafi, A.B.M.A.; Kumano, H.; Suemune, I.; Ok, Y.W.; Seong, T.Y. *CdO Epitaxial Layers Grown on (0 0 1) GaAs Surfaces by Metalorganic Molecular-Beam Epitaxy*; 2002; Vol. 237;.
21. Metz, A.W.; Ireland, J.R.; Zheng, J.G.; Lobo, R.P.S.M.; Yang, Y.; Ni, J.; Stern, C.L.; Dravid, V.P.; Bontemps, N.; Kannewurf, C.R.; et al. Transparent Conducting Oxides: Texture and Microstructure Effects on Charge Carrier Mobility in MOCVD-Derived CdO Thin Films Grown with a Thermally Stable, Low-Melting Precursor. *J Am Chem Soc* **2004**, *126*, 8477–8492, doi:10.1021/ja039232z.
22. Dantus, C.; Rusu, R.S.; Rusu, G.I. On the Mechanism of Electronic Transport in Polycrystalline CdO Thin Films. *Superlattices Microstruct* **2011**, *50*, 303–310, doi:10.1016/j.spmi.2011.07.008.
23. Taşçıoğlu, I.; Soylu, M.; Altındal, Ş.; Al-Ghamdi, A.A.; Yakuphanoglu, F. Effects of Interface States and Series Resistance on Electrical Properties of Al/Nanostructure CdO/p-GaAs Diode. *J Alloys Compd* **2012**, *541*, 462–467, doi:10.1016/j.jallcom.2012.07.001.
24. Abdulsattar, M.A.; Batros, S.S.; Adie, A.J. Spectroscopic Properties of Indium-Doped CdO Nanostructures Supported by DFT Calculations. *Surface Review and Letters* **2019**, *26*, 1850169.
25. Dakhel, A.A. Optoelectronic Properties of Eu- and H-Codoped CdO Films. *Current Applied Physics* **2011**, *11*, 11–15, doi:10.1016/j.cap.2010.06.003.
26. Turgut, G.; Aksoy, G.; İskenderoğlu, D.; Turgut, U.; Duman, S. The Effect of Eu-Loading on the Some Physical Features of CdO. *Ceram Int* **2018**, *44*, 3921–3928, doi:10.1016/j.ceramint.2017.11.183.

27. Dakhel, A.A. Transparent Conducting Properties of Samarium-Doped CdO. *J Alloys Compd* **2009**, *475*, 51–54, doi:10.1016/j.jallcom.2008.08.008.
28. Le, N.M.; Lee, B.T. Investigation of Material Properties and Defect Behavior in In-Doped CdO Films. *Appl Surf Sci* **2018**, *451*, 218–222, doi:10.1016/j.apsusc.2018.04.221.
29. Xie, M.; Zhu, W.; Yu, K.M.; Zhu, Z.; Wang, G. Effects of Doping and Rapid Thermal Processing in Y Doped CdO Thin Films. *J Alloys Compd* **2019**, *776*, 259–265, doi:10.1016/j.jallcom.2018.10.288.
30. Yakuphanoglu, F. Preparation of Nanostructure Ni Doped CdO Thin Films by Sol Gel Spin Coating Method. *J Solgel Sci Technol* **2011**, *59*, 569–573, doi:10.1007/s10971-011-2528-2.
31. Liu, C.P.; Foo, Y.; Kamruzzaman, M.; Ho, C.Y.; Zapien, J.A.; Zhu, W.; Li, Y.J.; Walukiewicz, W.; Yu, K.M. Effects of Free Carriers on the Optical Properties of Doped CdO for Full-Spectrum Photovoltaics. *Phys Rev Appl* **2016**, *6*, 1–12, doi:10.1103/PhysRevApplied.6.064018.
32. Soylu, M.; Al-Ghamdi, A.A.; Yakuphanoglu, F. Transparent CdO/n-GaN(0001) Heterojunction for Optoelectronic Applications. *Journal of Physics and Chemistry of Solids* **2015**, *85*, 26–33, doi:10.1016/j.jpcs.2015.04.015.
33. Li, E.; Qin, K.; Shen, Y.; Ma, D.; Yuan, P.; Wang, H.; Cui, Z. Self-Powered Photodetector with High Photocurrent and Polarization Sensitivity Based on the GaN/CdO Heterostructure. *Journal of Physical Chemistry C* **2025**, doi:10.1021/acs.jpcc.5c00597.
34. Moutinho, H.R.; Hasoon, F.S.; Abulfotuh, F.; Kazmerski, L.L. Investigation of Polycrystalline CdTe Thin Films Deposited by Physical Vapor Deposition, Close-spaced Sublimation, and Sputtering. *Journal of Vacuum Science & Technology A* **1995**, *13*, 2877–2883, doi:10.1116/1.579607.
35. Li, K.; Tang, R.; Zhu, C.; Chen, T. Critical Review on Crystal Orientation Engineering of Antimony Chalcogenide Thin Film for Solar Cell Applications. *Advanced Science* **2024**, *11*, 2304963, doi:10.1002/ADVS.202304963.
36. Dakhel, A.A. Bandgap Narrowing in CdO Doped with Europium. *Opt Mater (Amst)* **2009**, *31*, 691–695, doi:10.1016/J.OPTMAT.2008.08.001.
37. Waseda, Y.; Matsubara, E.; Shinoda, K. X-Ray Diffraction Crystallography. *X-Ray Diffraction Crystallography* **2011**, doi:10.1007/978-3-642-16635-8.
38. Khalaf, A.; Matar, M.; Abdeen, W. Tunable Band Gap and Antiferromagnetic Ordering in Co-Doped CdO Nanostructures. *J Supercond Nov Magn* **2021**, *34*, 2911–2921, doi:10.1007/s10948-021-05973-0.
39. Ravikumar, M.; Ganesh, V.; Shkir, M.; Chandramohan, R.; Arun Kumar, K.D.; Valanarasu, S.; Kathalingam, A.; AlFaify, S. Fabrication of Eu Doped CdO [Al/Eu-NCdO/p-Si/Al] Photodiodes by Perfume Atomizer Based Spray Technique for Opto-Electronic Applications. *J Mol Struct* **2018**, *1160*, 311–318, doi:10.1016/j.molstruc.2018.01.095.
40. Munawar, T.; Iqbal, F.; Yasmeen, S.; Mahmood, K.; Hussain, A. Multi Metal Oxide NiO-CdO-ZnO Nanocomposite–Synthesis, Structural, Optical, Electrical Properties and Enhanced Sunlight Driven Photocatalytic Activity. *Ceram Int* **2020**, *46*, 2421–2437, doi:10.1016/j.ceramint.2019.09.236.

41. Venkata Reddy, C.; Shim, J.; Byon, C.; Krishna Rao, L. V.; Satish, D. V.; Ravikumar, R.V.S.S.N. Room Temperature Synthesis and Spectral Characterization of Cu²⁺-Doped CdO Powder. *Indian Journal of Physics* **2016**, *90*, 359–364, doi:10.1007/s12648-015-0753-1.
42. Zargar, R.A.; Shah, A.H.; Arora, M.; Mir, F.A. Crystallographic, Spectroscopic and Electrical Study of ZnO:CdO Nanocomposite-Coated Films for Photovoltaic Applications. *Arab J Sci Eng* **2019**, *44*, 6631–6636, doi:10.1007/s13369-019-03823-9.
43. Abou-Ras, D.; Kirchartz, T. Electron-Beam-Induced Current Measurements of Thin-Film Solar Cells. *ACS Appl Energy Mater* **2019**, *2*, 6127–6139.
44. Hubbard, W.A.; Mecklenburg, M.; Chan, H.L.; Regan, B.C. STEM Imaging with Beam-Induced Hole and Secondary Electron Currents. *Phys Rev Appl* **2018**, *10*, doi:10.1103/PhysRevApplied.10.044066.
45. Mecklenburg, M.; Hubbard, W.A.; Lodico, J.J.; Regan, B.C. Electron Beam-Induced Current Imaging with Two-Angstrom Resolution. *Ultramicroscopy* **2019**, *207*, doi:10.1016/j.ultramic.2019.112852.
46. Chernyak, L.; Schwarz, C.; Flitsiyan, E.S.; Chu, S.; Liu, J.L.; Gartsman, K. Electron Beam Induced Current Profiling of ZnO P-n Homojunctions. *Appl Phys Lett* **2008**, *92*, doi:10.1063/1.2896613.
47. Przewdziecka, E.; Stachowicz, M.; Chusnutdinow, S.; Jakieła, R.; Kozanecki, A. Electron Beam Induced Current Profiling of the P-ZnO:N/n-GaN Heterojunction. *Appl Phys Lett* **2015**, *106*, 062106, doi:10.1063/1.4908291.
48. Osinsky, A.; Dong, J.W.; Kauser, M.Z.; Hertog, B.; Dabiran, A.M.; Chow, P.P.; Pearton, S.J.; Lopatiuk, O.; Chernyak, L. MgZnO/AlGaIn Heterostructure Light-Emitting Diodes. In *Proceedings of the Applied Physics Letters*; November 8 2004; Vol. 85, pp. 4272–4274.
49. Alivov, Y.I.; Xiao, B.; Akarca-Biyikli, S.; Fan, Q.; Morkoç, H.; Johnstone, D.; Lopatiuk-Tirpak, O.; Chernyak, L.; Litton, W. Properties of Isotype N-ZnO/n-GaN Heterostructures Studied by I-V-T and Electron Beam Induced Current Methods. *Journal of Physics Condensed Matter* **2008**, *20*, doi:10.1088/0953-8984/20/8/085201.
50. I.D. Makuta; S.K. Poznyak; A.I. Kulak Makuta 1990. *Solid State Commun* **1990**, *76*, 65–68, doi:https://doi.org/10.1016/0038-1098(90)90298-P.
51. Oakes, J.J.; Greenfield, I.G.; Partain, L.D. Diffusion Length Determination in Thin-Film Cu_xS/CdS Solar Cells by Scanning Electron Microscopy. *Journal of Applied Physics* **1977**, *48*, 2548–2555, doi:10.1063/1.323971.
52. Chusnutdinow, S.; Szot, M.; Wojtowicz, T.; Karczewski, G. PbSe/CdTe Single Quantum Well Infrared Detectors. *AIP Adv* **2017**, *7*, doi:10.1063/1.4978527.